Progress In Electromagnetics Research B, Vol. 61, 225–239, 2014

Design and Implementation of a Compact Practical Passive Beam-Forming Matrix for 3D S-Band Radar

Hamid M. Sadeghi, Mehdi Moradianpour, Maziar Hedayati*, Gholamreza Askari, and Parisa Moslemi

Abstract—In this paper a compact two-layer microstrip passive beam-forming matrix in the 2.9–3.1 GHz frequency band is designed, fabricated, and measured. This 13×6 matrix is a passive circuit that can transform the 13 patterns of an antenna array into six possible beams to decrease the complexity for multiplexing/demultiplexing operation in three dimensional Radar. The 90 degrees hybrid couplers with high isolation between two signals and phase shifters between the couplers are used to provide proper signals in outputs. The matrix structure consists of metal walls around transmission lines to eliminate the surface waves. Also, a coaxial to microstrip transition is used to extract accurate measurement results. A special box is designed to cover matrix which has many design considerations such as cutoff frequency, destructive effects on couplers and other parts of matrix, and all of these effects are analyzed and considered to achieve the optimum performance in this paper. The matrix is designed on a substrate Rogers RT5880 with $\varepsilon_r = 2.2$, substrate height = 0.787 mm, and loss tangent = 0.0009. Also the thickness of the copper cladding layer is 17 µm. The maximum amplitude and phase errors in outputs are 0.6 dB and 7°, respectively, and VSWRs are less than 1.35 in the matrix bandwidth with at least 20 dB isolation between all ports.

1. INTRODUCTION

Multibeam and beam-scanning antennas are crucial to the modern communication systems. Many applications, such as local area networks, satellites, and surveillance systems require wide angle coverage. In general, the main beam of an antenna is steered by properly adjusting the phase and the amplitude of the radiating elements. The amplitude and phase distributions are typically imposed by using beam-forming networks (BFNs). The important classes of these multiple beamforming networks such as Butler Matrix (circuit-based beamformer), Rotman Lens (lens-based beamformer), and integrated reflector systems form microwave passive networks [1–5]. The Rotman Lens is an attractive beamforming network due to its low cost, reliability, simplicity, and wide angle scanning capabilities [6–9], whereas the most popular circuit-based BFNs are Blass, Nolen, and Butler matrix [10–12]. All these solutions offer multiple-beam or beam-scanning capabilities by selecting one or several input/output ports, or mechanically displacing a moving feed. Circuit-based BFNs are designed by using simple building blocks, such as power dividers, directional couplers, phase shifters, and crossovers. The most common BFNs, used recently due to its easy fabrication process and low cost, is Butler matrix which is used for the antenna array feed. It requires N input ports (N beams), N output ports, $(N/2)\log2(N)$ hybrid couplers, and $(N/2)\log2(N-1)$ fixed phase shifters to form the $N \times N$ network [13–15]. Also, the output ports are spaced in such a way that the elements of the antenna array can be directly attached to the network.

Received 14 September 2014, Accepted 13 November 2014, Scheduled 3 December 2014

* Corresponding author: Maziar Hedayati (maziarhedayati2020@gmail.com).
The authors are with the Information and Communication Technology Institute (ICTI), Isfahan University of Technology (IUT), Isfahan 84156, Iran.

Most surveillance radars are two-dimensional (2D) arrays, measuring only range and azimuth coordinates of targets [16–19]. More recent three-dimensional (3D) radar designs use a single antenna to measure all three coordinates. For example, a stacked beam antenna consists of a number of stacked beams in elevation in the receive mode and a single broad-coverage elevation beam in the transmit mode [20–26]. To have a suitable coverage in elevation pattern, CSC2 coverage is needed. On the other hand, the resolution of height finding in the three-dimensional Radars impose to have the narrow elevation beam width specially near the horizon (around 1 degree) which is possible with the excitation of multi narrow beams. But low complexity and simple structure are the most important criteria in three-dimensional Radars, so it is necessary to use a special combination of the stacked beams to create the appropriate patterns for height finding. In this paper, a matrix is designed to transform 13 beams of an antenna to 6 desired beams for height finding which is not possible with previous reported passive networks in the literatures. The remainder of this paper is organized as follows. In Section 2, the synthesis of beamforming network and configuration of the matrix and its design formulation are presented. In addition, the design of appropriate couplers and phase shifters, based on the approach presented in [27, 28] is described. The matrix is designed on a two-layer microstrip to achieve miniaturization. A critical problem for the performance of matrices is surface waves in microstrip circuits which can disturb the couplers behavior [29–32]. In Section 3, discussions and solutions to overcome the surface waves losses are presented. A coaxial-to-microstrip transition is required for planner structures to extract accurate measurement results, which is discussed in Section 4. In Section 5, a special box is designed to help better performance of the matrix over the frequency band width. The experimental results are given in Section 6. Finally Section 7 concludes the paper.

2. THE SYNTHESIS OF THE BEAM FORMING NETWORK

There are various methods such as phase array antenna, multi-feed reflector antennas (MFRAs), and nodding techniques to obtain desired radiation patterns of antennas for different applications in radar systems and satellite communications. Using multi-feed reflector antennas has been extensively investigated in recent years for pattern synthesis. Their advantages are simple geometry, ease of fabrication, better cross polarization, frequency reuse and higher reliability [33]. The most important application of MFRAs is height finding, so this type of antenna is used in this paper. The antenna geometry is shown in Fig. 1(a). The reflector antenna is a paraboloid of revolution with elliptic cross-section from front view. Reflector aperture is 4.27 m high by 6.20 m wide with focal axis of 2.6 m. The reflector is illuminated by 15 horn antennas, which has been moved progressively back from the focal plane. This number of feed horns for antenna is chosen to have 20 degree elevation coverage. To reduce the complexity, the outputs of the first three horns (#1-1, #1-2, #1-3) are combined and create ($J1$). The horns are placed in a line contour which follows the reflector curvature. According to the geometrical optic principal, the pattern of channel #1($J1$) is used to illuminate the targets in near zone, but the pattern of horn 13($J13$) illuminates the angles near the ground in far zone. The 13 primary patterns of antenna are shown in Fig. 1(b). But in three-dimensional Radar, the high accurate angular resolution is necessary to find targets in the far distance and less resolution for targets close to the Radar. So narrow beam and high gain (around 1 degree) for far zone and wide beam and lower gain (around 7.8 degree) for near zone are required. To satisfy these requirements, a special combination of patterns is necessary. For example, the narrowest beam (B_6) must be the combination of the five patterns ($J_9 - J_{13}$) to cover the long distance (near the horizon). So according to above discussion, a special combination to satisfy a desired coverage pattern shown in Fig. 1(c) is selected which are presented in the set of Equation (1).

$$\begin{cases} B_1\,(J_{14}): & J_1,\ J_2 \\ B_2\,(J_{15}): & J_2,\ J_3 \\ B_3\,(J_{16}): & J_3,\ J_4,\ J_5 \\ B_4\,(J_{17}): & J_4,\ J_5,\ J_6,\ J_7,\ J_8 \\ B_5\,(J_{18}): & J_6,\ J_7,\ J_8,\ J_9,\ J_{10},\ J_{11},\ J_{12} \\ B_6\,(J_{19}): & J_9,\ J_{10},\ J_{11},\ J_{12},\ J_{13} \end{cases} \tag{1}$$

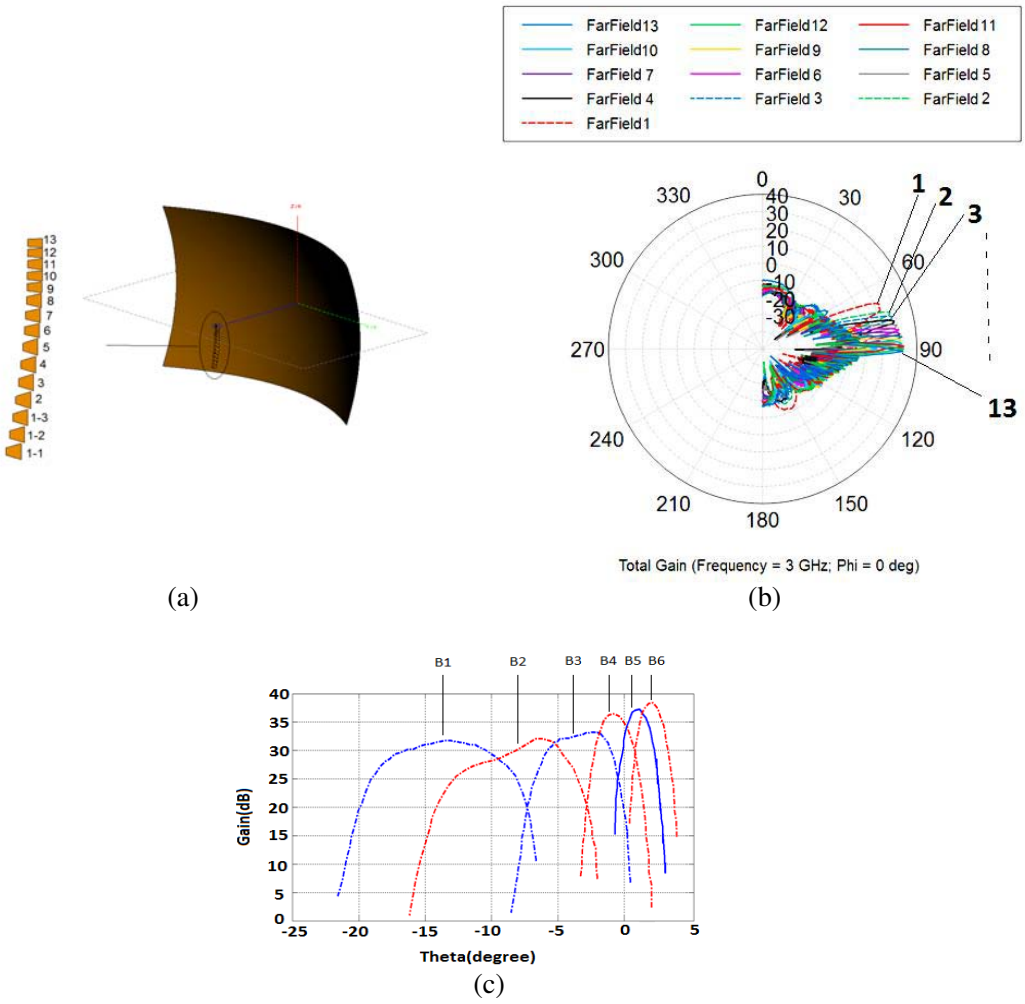

Figure 1. (a) Antenna geometry in FEKO. (b) The 13 primary beams. (c) The six desired patterns.

where B_i $(i = 1 : 5)$ are the six desired patterns, and J_i $(i = 1 : 13)$ are the input signals from horn antennas. These desired patterns are calculated to have about 500 m accuracy in height finding. To synthesize the desired radiation patterns, the optimization tool in FEKO with genetic algorithm method has been used to find the excitation of radiating elements of MFRAs. The final amplitudes and phases are listed in Table 1.

Now according to equation set (1), it is possible to introduce a block diagram which is shown in Fig. 2 where the rectangles and lines are directional couplers and transmission lines, respectively. The phase of the signals is satisfied by the line passive phase shifters which are implemented in the circuit. To simplify, all of the couplers in the first column (1–11) are 3 dB hybrid. The presented matrix consists of 29 single-section coupled-line directional couplers.

According to Fig. 2, the inputs-outputs relations can be formulated as Equations (2)–(7).

$$B_1 = c_{12} \cdot J_1 + \frac{1}{\sqrt{2}} \cdot t_{12} \cdot J_2 \tag{2}$$

$$B_2 = \frac{1}{\sqrt{2}} \cdot c_{13} \cdot J_2 + \frac{1}{\sqrt{2}} \cdot t_{13} \cdot J_3 \tag{3}$$

$$B_3 = \frac{1}{\sqrt{2}} \cdot c_{21} \cdot J_3 + \frac{1}{\sqrt{2}} \cdot t_{17} \cdot t_{21} \cdot J_4 + \frac{1}{\sqrt{2}} \cdot c_{17} \cdot t_{21} \cdot J_5 \tag{4}$$

$$B_4 = \frac{1}{\sqrt{2}} \cdot c_{14} \cdot c_{28} \cdot J_4 + \frac{1}{\sqrt{2}} \cdot t_{14} \cdot c_{28} \cdot J_5 + \frac{1}{\sqrt{2}} \cdot t_{26} \cdot t_{28} \cdot J_6 + \frac{1}{\sqrt{2}} \cdot t_{24} \cdot c_{26} \cdot t_{28} \cdot J_7 + \frac{1}{\sqrt{2}} \cdot c_{24} \cdot c_{26} \cdot t_{28} \cdot J_8 \quad (5)$$

$$B_5 = \frac{1}{\sqrt{2}} \cdot c_{18} \cdot c_{20} \cdot c_{29} \cdot J_6 + \frac{1}{\sqrt{2}} \cdot t_{18} \cdot c_{20} \cdot c_{29} \cdot J_7 + \frac{1}{\sqrt{2}} \cdot t_{20} \cdot c_{29} \cdot J_8 + \frac{1}{\sqrt{2}} \cdot t_{25} \cdot t_{29} \cdot J_9 + \frac{1}{\sqrt{2}} \cdot t_{22} \cdot c_{25} \cdot t_{29} \cdot J_{12} \quad (6)$$

$$B_6 = \frac{1}{\sqrt{2}} \cdot c_{19} \cdot c_{27} \cdot J_9 + \frac{1}{\sqrt{2}} \cdot t_{19} \cdot c_{27} \cdot J_{10} + \frac{1}{\sqrt{2}} \cdot t_{23} \cdot t_{27} \cdot J_{11} + \frac{1}{\sqrt{2}} \cdot t_{25} \cdot t_{16} \cdot t_{23} \cdot t_{27} \cdot J_{12} + c_{16} \cdot c_{23} \cdot t_{27} \cdot J_{13} \quad (7)$$

where c_{ij} denotes the coupling coefficient and t_{ij} the transmission coefficient. Considering the signal values of Table 1 and Equations (2) to (7), the coupling and transmission coefficients are calculated. The final couplers coefficients are listed in Table 2.

Table 1. Desired signals values at 3 GHz.

J_{14}	J_1 = –4 dB Phase = –23	J_2 = –5.2 dB Phase = –19		
J_{15}	J_2 = –6.4 dB Phase = –10	J_3 = –5.9 dB Phase = –10		
J_{16}	J_3 = –9 dB Phase = 147	J_4 = –6.7 dB Phase = 147	J_5 = –9 dB Phase = 147	
J_{17}	J_4 = –12.9 dB Phase = –125	J_5 = –9.1 dB Phase = –125	J_6 = –8.8 dB Phase = –125	J_7 = –9.7 dB Phase = –125 J_8 = –15 dB Phase = –125
J_{18}	J_6 = –16.5 dB Phase = 24 J_7 = –10.9 dB Phase = 24	J_8 = –8.5 dB Phase = 24 J_9 = –10.9 dB Phase = 24	J_{10} = –12.3 dB Phase = 24 J_{11} = –13.2 dB Phase = 20	J_{12} = –16.7 dB Phase = 27
J_{19}	J_9 = –14.5 dB Phase = –155	J_{10} = –10.9 dB Phase = –145	J_{11} = –9.6 dB Phase = –145 J_{12} = –9.6 dB Phase = –138	J_{13} = –6.8 dB Phase = –145

Table 2. Value of couplers coefficients.

N	**1**	**2**	**3**	**4**	**5**	**6**	**7**
C (dB)	2.64	3.23	2.88	3.3	3.3	2.82	2.88
t (dB)	3.41	2.87	3.23	2.8	2.8	3.43	3.31
N	**9**	**10**	**11**	**12**	**13**	**14**	**15**
C (dB)	2.9	2.9	2.9	2.4	2.96	4.06	6.22
t (dB)	3.3	3.3	3.3	3.825	3.15	2.22	1.26
n	**17**	**18**	**19**	**20**	**21**	**22**	**23**
C (dB)	5.5	3.8	4.05	2.85	2.9	4.62	5.55
t (dB)	1.55	2.39	2.24	3.29	3.2	1.96	1.53
n	**25**	**26**	**27**	**28**	**29**		
C (dB)	3	3	3.31	4.2	3.7		
t (dB)	3.35	3.15	2.78	2.16	2.5		

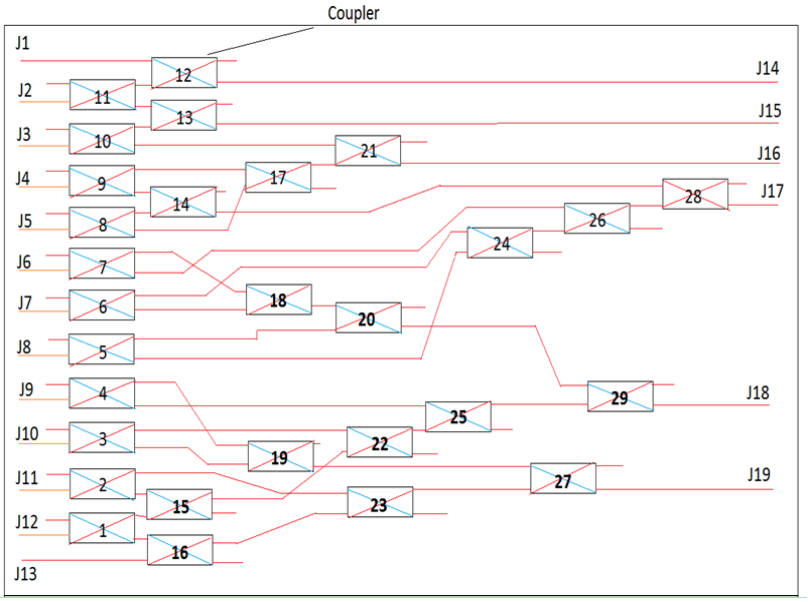

Figure 2. Block diagram of matrix (The rectangulars are couplers).

3. SURFACE WAVED PROBLEM AND ITS SOLUTION

The use of microstrip as a transmission line has demanded a deeper knowledge of the behavior of the microstrip discontinuities. The substrate surface waves in discontinuities is a topic that has been recently considered. The concept of substrate surface waves is evident when it is considered that the dielectric substrate with its ground plane is capable of supporting the dielectric slab type modes. Thus at any discontinuity in the conducting microstrip line and particulary at an open circuit termination, the substrate surface waves will be launched. The surface waves destroy the isolation between the microstrip circuits. From some practical stand points, the existence and elimination of these substrate surface waves should be considered for the matrix applications. This section has introduced a method to eliminate the surface waves in the matrix which can disturb the accuracy of the matrix in the height finding operations. Mode conversion from the microstrip mode to the surface wave mode is a common way of the surface wave losses. Propagating parameters and the cutoff frequency of the surface waves are obtained with Maxwell equations. Fig. 3 illustrates the cross section of the structure. The surface waves can be propagated in such structures. TM_0 is the dominant mode with the cutoff frequency of zero. Performance of this mode in low frequencies is similar to the TEM mode. TM_1 is the next mode in the structure in which its cut off frequency is obtained by Equation (8).

$$\tan\left(\sqrt{\varepsilon_r} \times K_0 \times a\right) = -\sqrt{\varepsilon_r} \tan\left(K_0 \times c\right) \tag{8}$$

where $K_0 = (\frac{2\pi f}{V})$ and V is the speed of the wave in vacuum. In regard to Equation (8) and the characteristic of the dielectric ($\varepsilon_r = 2.2$, $a = 0.787\,\text{mm}$, $c = 7\,\text{mm}$), the cut off frequency of TM_1 is 10.71 GHz which is out of the matrix operation frequencies. So TM_1 is not challengeable for the matrix. Several vias or conductor walls between the strips and the ground are used to eliminate the mode conversion of TM_0. A part of the microstrip line is shown in Fig. 3 with metal walls which can be replaced with the vias. The result of these structures is shown in Fig. 4. By selecting an appropriate distance between the walls and transmission lines obtained by the optimization in HFSS 13, the mode conversion is eliminated. Fig. 4 shows that the walls eliminate the mode conversion and decrease the loss consequently. S_{21} parameter of the structure with the metal walls is 0.16 dB which is better than that without the metal walls. However, the improvement in transmission coefficient by using metal walls is only 0.06 dB, but that modification is just for a part of circuit, and the total improvement is considerable. The vias cannot eliminate the surface waves as well as the metal walls, but it can decrease a part of the surface waves and modify the behavior of the matrix.

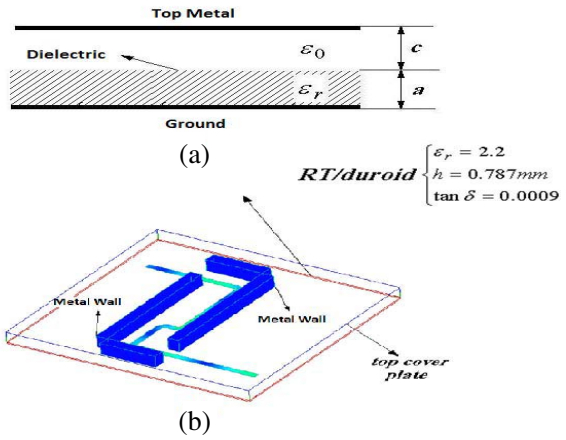

Figure 3. (a) The cross section of structure. (b) Metal walls around transmission lines.

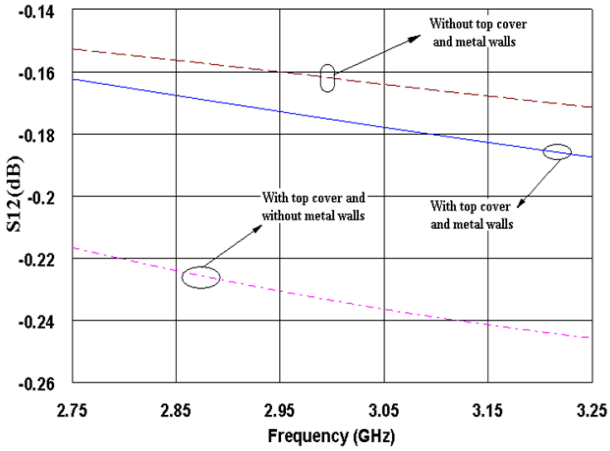

Figure 4. Simulation result of transmission line with and without walls.

4. THE COAXIAL TO MICROSTRIP TRANSITION

A coaxial to microstrip transition is required in the most planar structures to extract accurate measurement results. The coaxial to microstrip transition must support only a single propagation mode over a desired frequency bandwidth. The first consideration in design of transition is impedance matching, so the coaxial and microstrip line are designed to be 50 Ω. But having the same characteristic impedance does not always guarantee a good transition between two transmission lines, and the field distributions of the transmission line must also be matched. Therefore, the metal wall around the feed point is used as an interface to match the electromagnetic field distributions at coaxial to microstrip transitions which is shown in Fig. 5(a). To study the effects of the metal wall on the transition, the insertion loss and reflection coefficient of feed point with and without wall are plotted in Figs. 5(b), (c). As shown in Fig. 5(b), the transition with the wall has return loss better than −22 dB which is 10 dB better than the transition without walls, and the insertion loss is decreased around 0.8 dB in 3 GHz which is shown in Fig. 5(c).

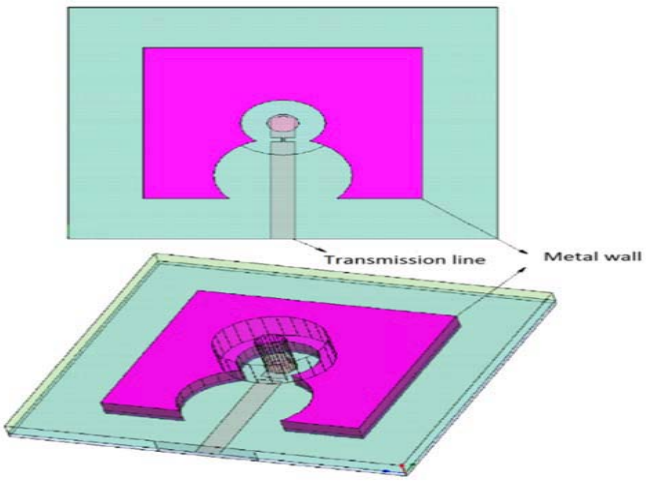

(a)

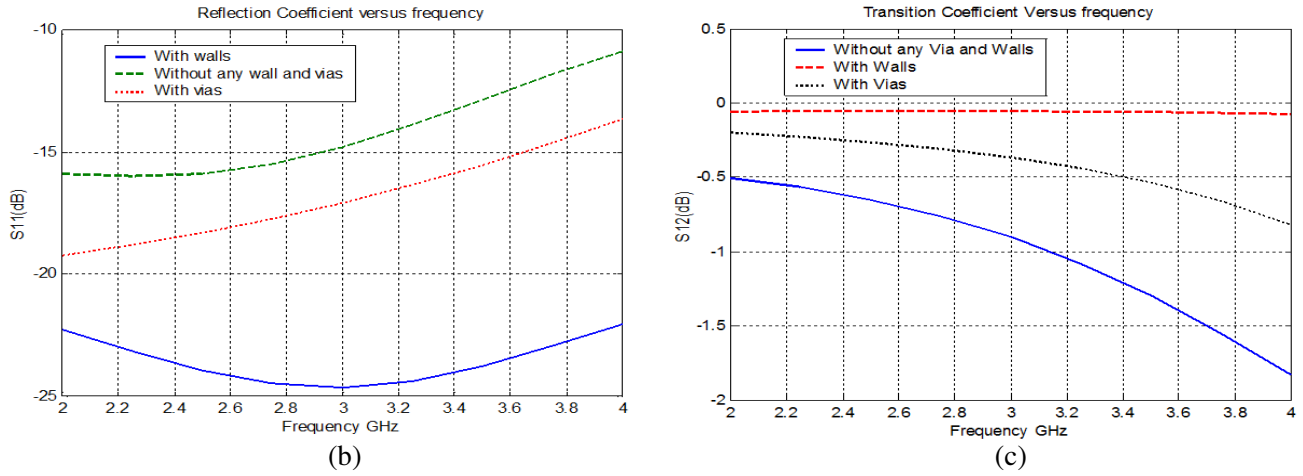

Figure 5. The effects of walls on transition. (a) Metal walls around probe. (b) Reflection coefficient. (c) Transmission coefficient.

5. BOX CONSIDERATIONS DESIGN

5.1. Box Resonance

Finally, the matrix must be placed in a box. In order to eliminate the resonances of the box, there are several methods such as using an absorbing material over the box to reduce the quality factor of the resonances, using the extra elements to move away the box resonances, and shielding methods. In this paper, a shaped box is used for that purpose. Fig. 6 shows the top view of the boxes. According to Fig. 6(a), the reflected wave from wall $\underline{a}(E_a^r)$ reaches wall $\underline{b}$. It is assumed that there is no loss in boxes, so $|E_a^r| = |E_b^i|$ where $|E_b^i|$ is the reflected wave from wall b. Amplitudes of E_a^r and E_b^i are equal, but they are different in phase (180 degrees). The phases of E_a^r and E_b^i should be the same in the first point to resonate. Therefore, the electrical length of the path in the box should be integer multiple of π (the length of path should be integer multiple of $\lambda/2$). In Fig. 6(b), the width of the box is reduced symmetrically. So the cutoff frequency of this part is more than the usual box. In this case, E_a^r and E_b^i vanish exponentially in the narrow part of the box, so the resonance frequency is moved to the higher frequency. As shown in Fig. 7(a), the resonance of the normal box is at 3 GHz, which disturbs performance of the matrix. But, with the new box, the unwanted resonances move to upper frequency than 4 GHz, illustrated in Fig. 7(b).

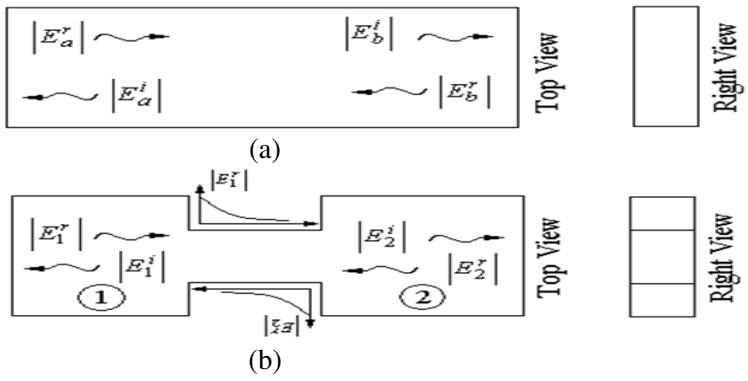

Figure 6. Box of matrix and wave tracing in box. (a) Normal box. (b) Shaped box.

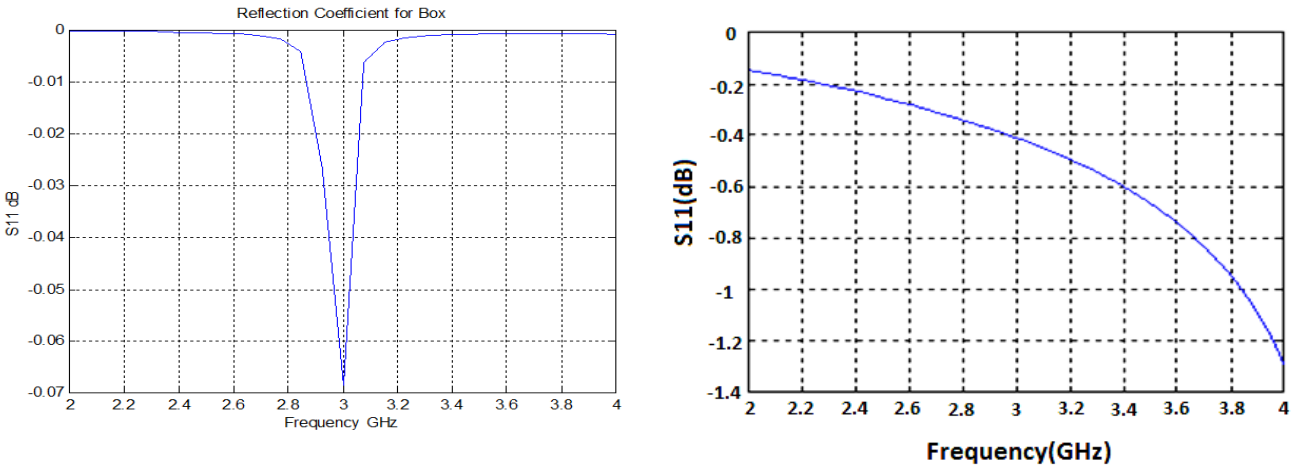

(a) (b)

Figure 7. Resonance frequency of box. (a) Primary box. (b) Shaped box.

5.2. Couplers Behavior inside the Box

The performance of the branch line couplers is investigated inside a box in this section. Fig. 8(a) shows a view of the branch line coupler in the box. In the simulation of the branch line without walls, there is a resonance in the bandwidth of the coupler, which must be removed. Two metal walls are placed around the coupler that construct a new waveguide with the box. The distance between the walls should be designed to construct the waveguide with the cutoff frequency higher than the coupler bandwidth. The S_{13} of the coupler inside the box with and without the walls are shown in Fig. 8(b). As shown, there is an unwanted resonance in the frequency bandwidth in the case of without walls which has been solved by using metal walls around the coupler. The S parameter of the coupler outside the box is plotted too which show close agreement with the S parameter of the coupler inside the box with the walls.

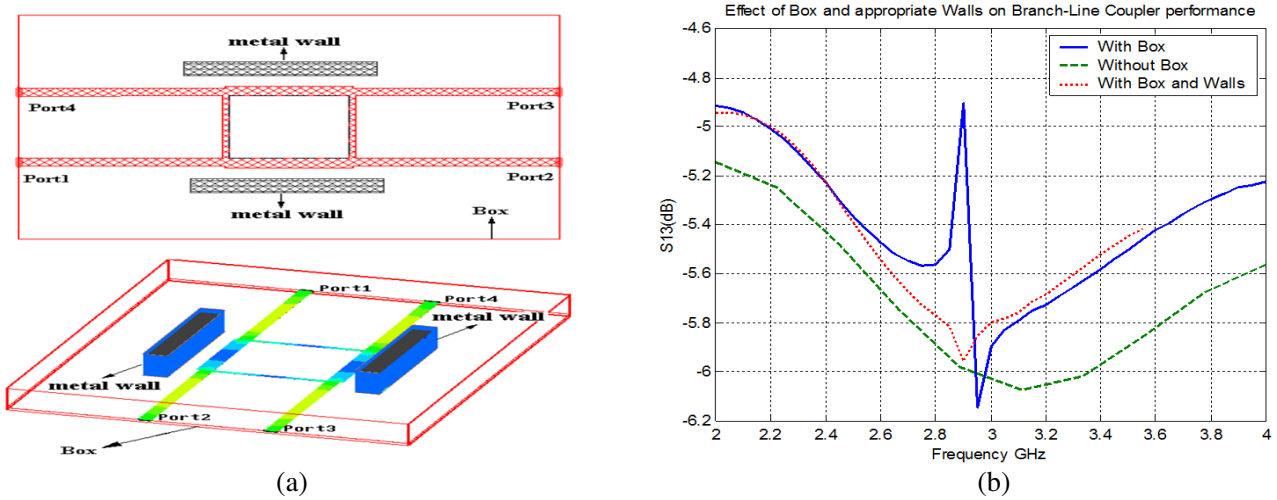

(a) (b)

Figure 8. Couplers behavior inside the box and S parameter of coupler with and without metal walls. (a) The coupler in the box. (b) S_{13}.

6. FINAL MATRIX DESIGN AND MEASUREMENT RESULT

6.1. Layout Considerations

Considering design procedure and all considerations in Parts 4 and 5, final design is implemented on a substrate Rogers RT Duroid5880 (0.787 mm thickness, $\varepsilon_r = 2.2$, and loss tangent = 0.0009), and the thickness of the copper cladding layer is 0.008 mm. This substrate is chosen because of its low loss tangent. Furthermore, the substrates with higher permittivity are more sensitive and have more frequency shift for certain fabrication tolerances. Another limitation, which can be imposed on the design is to predetermine the locations of the connectors. This means that the circuit layout must conform to the input and output locations. As a result, avoidance of bends cannot be kept in the inputs. The discontinuities such as bends are the causes of unwanted reflection in circuit, so it is desirable to reduce as many bends as possible. The layout of the designed 13×6 matrix is shown in Fig. 9.

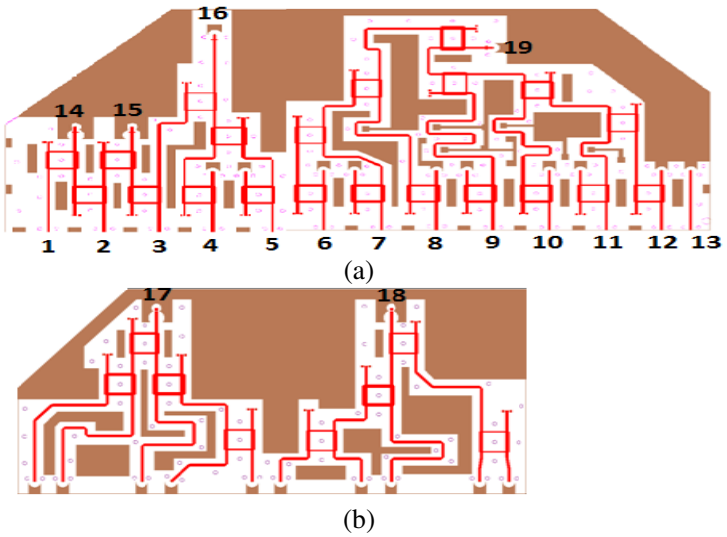

Figure 9. Layout of the designed broadband 13×6 matrix consisting of (a) bottom layer, (b) top layer.

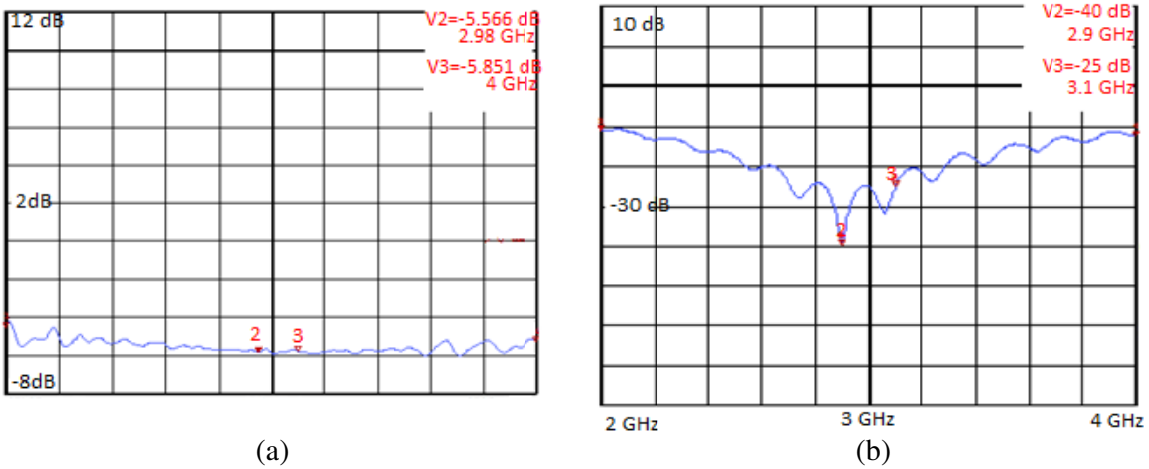

Figure 10. Measurement result of branch line coupler. (a) The coupling factor. (b) The return loss.

6.2. Simulation Method

Full wave analysis of this structure is very complex and is time consuming. So for simulation, to avoid full wave analysis, the structure is divided to several parts, and they are simulated separately. Then the S-parameters of all the parts are gathered, and the results of the matrix are obtained. The errors of fabrication are considerably difficult to simulate exactly. One way of getting around the problem is to

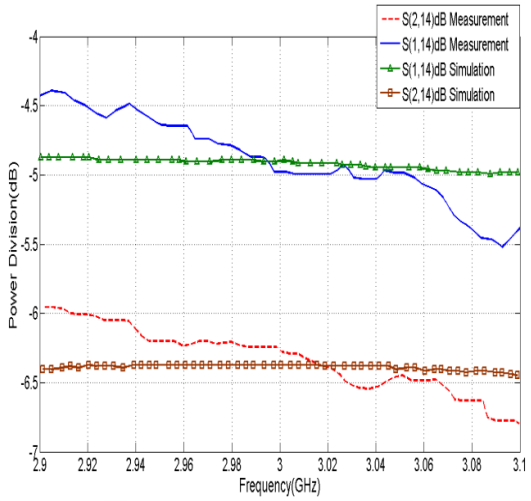

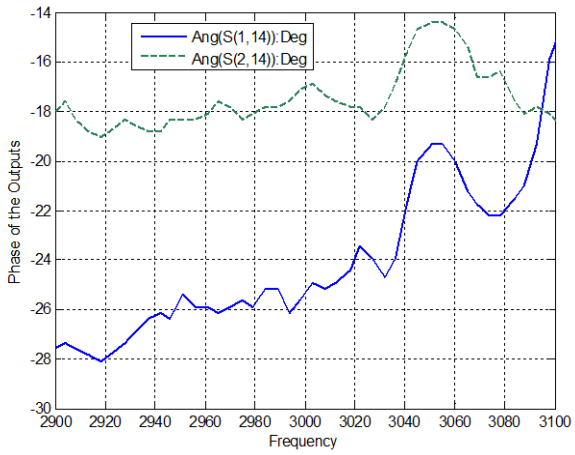

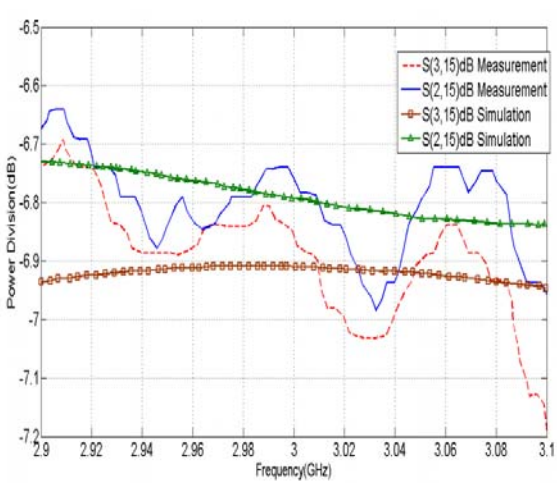

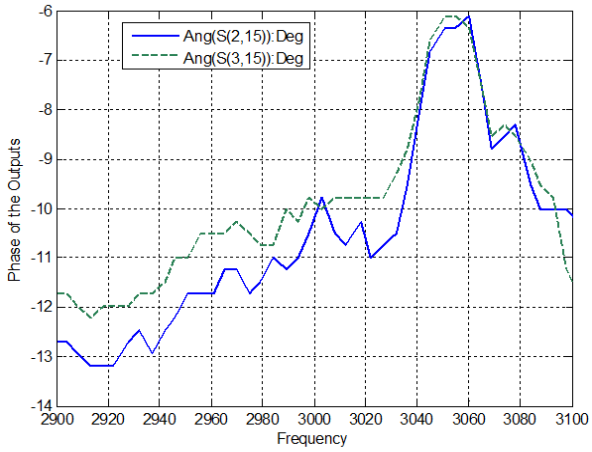

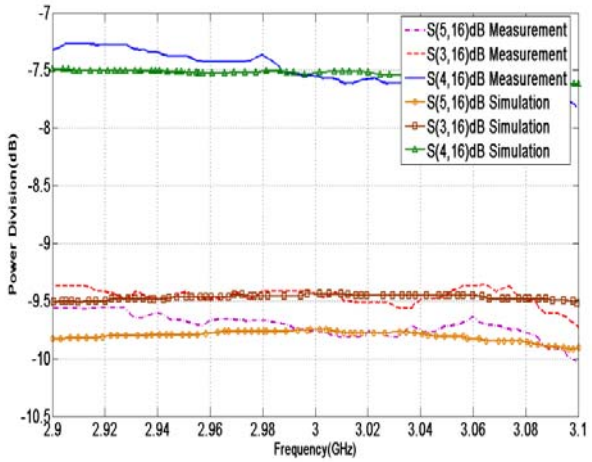

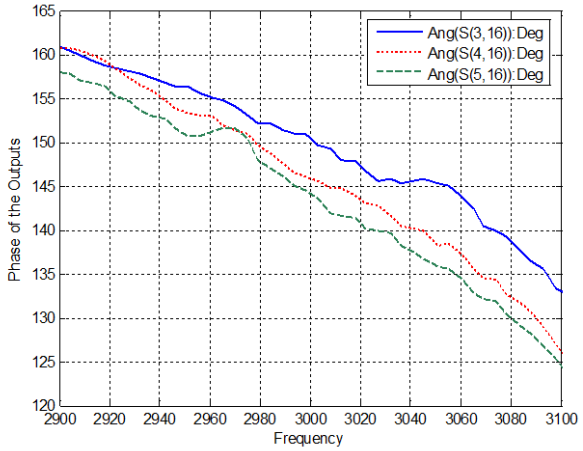

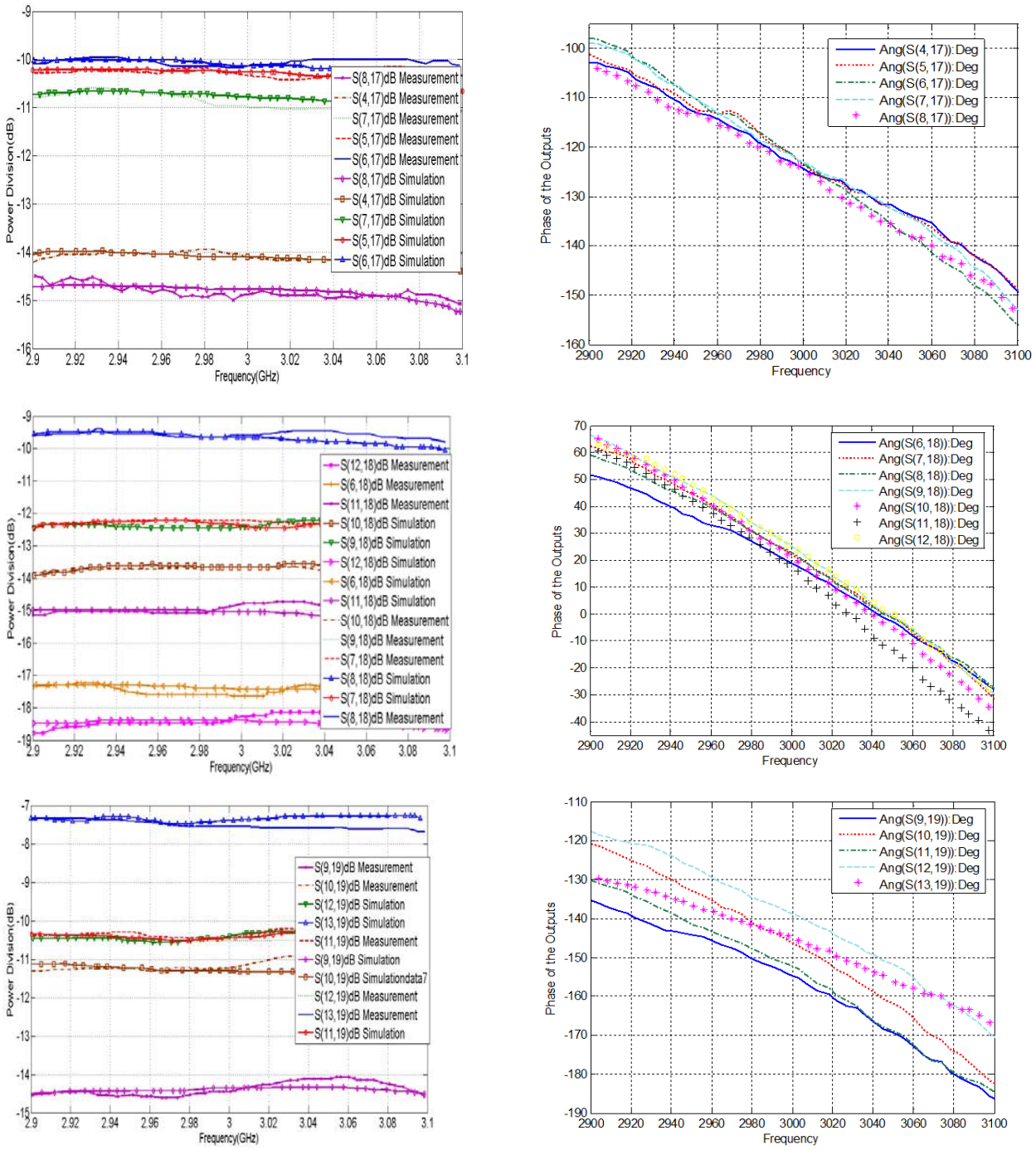

Figure 11. Measured amplitude and phase characteristics of the manufactured 13×6.

introduce these influences as random errors. Another solution is to consider the errors of manufacturing and verifying the simulation results from some implemented matrix components. For that purpose, some couplers were designed, fabricated, and measured. For instance, a branch line coupler with -5.5 dB coupling factor was designed, fabricated, and measured, and its measurement results are shown in Fig. 10. There was little difference between the measurement and simulation results in ADS 2009. So the simulation results of total matrix can be reliable. The measured data of the scattering matrix of

coupler can also be used for the total structure in the simulation. This method gives a high acceptable amplitude and phase output errors in the final measurements.

6.3. Measurement Results

The 13 × 6 matrix using coupled-line directional couplers has been designed, manufactured, and measured. The measured amplitude and phase characteristics of the manufactured 13 × 6 matrix are shown in Fig. 11. This measurement results are listed in Table 3. For instance, the amplitudes to produce the narrowest pattern for long distance search are −14.5 dB , −6.25 dB, −10.4 dB, −10.4 dB, and −7.4 dB at 3 GHz which have close agreement with the values in Table 1.

As shown in Table 3 in the center frequency of 3 GHz, the average amplitude and phase output unbalances are 1.65 dB and 4°, respectively, which are acceptable errors in outputs. The isolation between some of the output ports is shown in Fig. 12 and is better than 21 dB in 2900 GHz–3100 GHz which shows excellent matrix performances in its bandwidth. Fig. 13 illustrates that the VSWRs are less

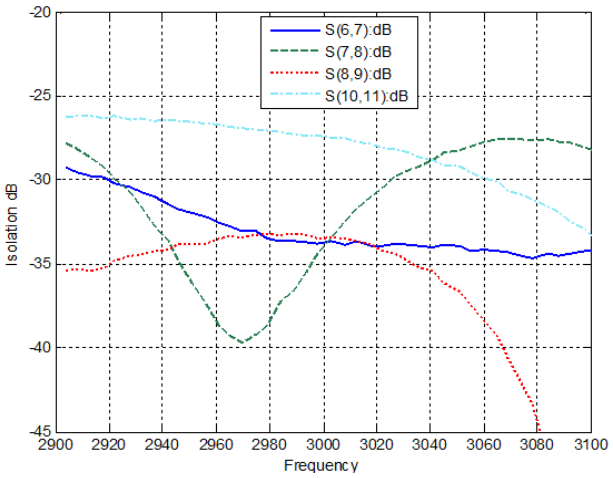

Figure 12. Measured isolation between some ports.

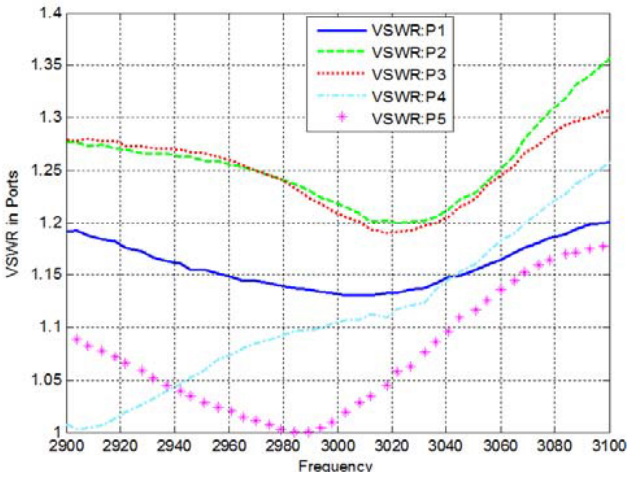

Figure 13. Measured VSWR.

Table 3. The measurement signal values at 3 GHz.

J_{14}	**J_1 = –5 dB Phase = –25**	**J_2 = –6.25 dB Phase = –17**		
J_{15}	J_2 = –6.75 dB Phase = –10	J_3 = –6.8 dB Phase = –10		
J_{16}	J_3 = –9.5 dB Phase = 150	J_4 = –7.55 dB Phase = 147	J_5 = –9.75 dB Phase = 144	
J_{17}	J_4 = –14 dB Phase = –125	J_5 = –10.4 dB Phase = –125	J_6 = –10.2 dB Phase = –125	J_7 = –11 dB Phase = –125 J_8 = –15 dB Phase = –125
J_{18}	J_6 = –17.7 dB Phase = 19 J_7 = –12.3 dB Phase = 24	J_8 = –9.6 dB Phase = 24 J_9 = –12.3 dB Phase = 27	J_{10} = –13.8 dB Phase = 24 J_{11} = –15 dB Phase = 20	J_{12} = –18.4 dB Phase = 27
J_{19}	J_9 = –14.5 dB Phase = –155	J_{10} = –11.3 dB Phase = –145	J_{11} = –10.4 dB Phase = –152 J_{12} = –10.4 dB Phase = –138	J_{13} = –7.4 dB Phase = –145

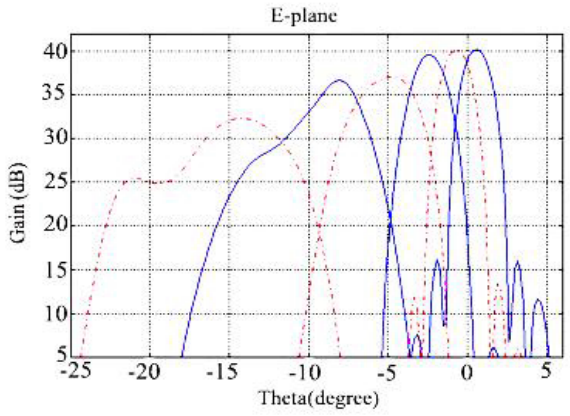

Figure 14. Calculated radiation pattern in elevation by using measured signals in Fig. 11.

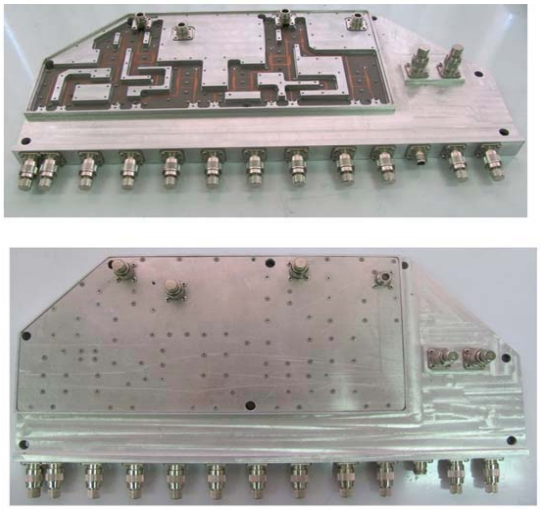

Figure 15. Outer view of fabricated matrix.

than 1.35. Also from Fig. 11 it is clear that in 2900 GHz–3100 GHz, the average amplitude and phase ripple of the transmission scattering parameters is less than 0.6 dB and 7°, respectively. To validate the matrix performance in the three-dimensional radar, the values of Table 3 are given in the horns input of Fig. 1(a). Fig. 14 shows the radiation patterns in the elevation angle at 3 GHz, which have close agreement with the desired pattern of Fig. 1(b). Fig. 15 shows the outer view of the fabricated matrix. Its physical dimensions are (26 cm × 57 cm), b (width) × L (length).

7. CONCLUSION

In this paper, a compact two-layer microstrip transceiver matrix in S-band for 3D radar is presented. The 90 degrees hybrid couplers with high isolation between two signals were fabricated, measured, and used to provide proper signals in matrix outputs. The surface wave and the box effects on the matrix performance were discussed and analyzed. To decrease the destructive effects of surface wave the metal walls around the transmission lines was used. To control the destructive effects of box around the matrix a special one was designed. The maximum amplitude and phase errors in outputs were 0.6 dB and 7°, respectively, and VSWR was less than 1.35 in the matrix bandwidth with 20 dB isolation between ports. To validate the matrix performance, the measured data were given to the antenna, and the obtained patterns were compared with the desired patterns which showed close agreement.

ACKNOWLEDGMENT

The authors would like to thank ICTI (Information and Communication Technology Institute) to provide the necessary facilities to fabricate and test of structure.

REFERENCES

1. Luneburg, R., *Mathematical Theory of Optics*, Brown Univ., Providence, RI, USA, 1944.
2. Rotman, W. and R. F. Turner, "Wide-angle microwave lens for linesource applications," *IEEE Trans. Antennas Propag.*, Vol. 11, No. 11, 623–632, Nov. 1963.
3. Mazzolla, V. and J. E. Becker, "Coupler-type bend for pillbox antennas," *IEEE Trans. Microw. Theory Techn.*, Vol. 15, No. 8, 462–468, Aug. 1967.

4. Ettorre, M., R. Sauleau, and L. Le Coq, "Multi-beam multi-layer leaky wave SIW pillbox antenna for millimeter-wave applications," *IEEE Trans. Antennas Propag.*, Vol. 59, No. 4, 1093–1100, Apr. 2011.
5. Ettorre, M., R. Sauleau, L. Le Coq, and F. Bodereau, "Single-folded leaky-wave antennas for automotive radars at 77 GHz," *IEEE Antennas Wireless Propag. Lett.*, Vol. 9, 859–862, Sep. 2010.
6. Dong, J., A. I. Zaghloul, R. Sun, C. J. Reddy, and S. J. Weiss, "Rotman lens amplitude, phase, and pattern evaluations by measurements and full wave simulations," *Appl. Comput. Electromagn. (ACES) J.*, Vol. 24, No. 6, 267–276, 2009.
7. Dong, J., A. I. Zaghloul, and R. Rotman, "Non-focal minimum phase-error planar Rotman lenses," *URSI National Radio Science Meeting*, Colorado, 2008.
8. Dong, J. and A. I. Zaghloul, "Method and computer aided investigation of microwave lens for 360-degree scanning," *IEEE Int. Symp. on Antennas Propagation*, Charleston, SC, 2009.
9. Dong, J. and A. I. Zaghloul, "Implementation of microwave lens for 360-degree scanning," *IEEE Int. Symp. on Antennas Propagation*, Charleston, SC, 2009.
10. Blass, J., "Multidirectional antenna — A new approach to stackedbeams," *IRE Int. Convention Rec.*, Vol. 8, 48–50, New York, USA, Mar. 1966.
11. Fonseca, N. J. G., "Printed-band 4×4 Nolen matrix for multiple beam antenna applications," *IEEE Trans. Antennas Propag.*, Vol. 57, No. 6, 1673–1678, Jun. 2009.
12. Butler, J. and R. Lowe, "Beam forming matrix simplifies design of electronically scanned antennas," *Electron. Design*, Vol. 9, 170–173, Apr. 1961.
13. Moody, H. J., "The systematic design of the Butler matrix," *IEEE Trans. Antennas Propag.*, Vol. 12, No. 6, 786–788, Nov. 1964.
14. Foster, H. E. and R. E. Hiatt, "Butler network extension to any number of antenna ports," *IEEE Trans. Antennas Propag.*, Vol. 18, No. 6, 818–820, Nov. 1970.
15. Ohira, T. and K. Gyoda, "Hand-held microwave direction-of-arrival finder based on varactor-tuned analog aerial beamforming," *Asia-Pacific Microwave Conference*, 585–588, Dec. 3–6, 2001.
16. Parvazi, P., A. B. Gershman, and Y. I. Abramovich, "Detecting outliers in the estimator bank-based direction finding techniques using the likelihood ratio quality assessment," *IEEE International Conference on Acoustics, Speech and Signal Processing*, Vol. 2, II-1065–II-1068, Apr. 15–20, 2007.
17. Bellion, A., C. Le Meins, A. Julien-Vergonjanne, and T. Monediere, "Generation of calibration tables for direction finding antennas using FEKO," *24th Annual Review of Progress in Applied Computational Electromagnetics*, 903–908, Mar. 2008.
18. Gething, P. J. D., "High-frequency direction finding," *Proceedings of the Institution of Electrical Engineers*, Vol. 113, No. 1, 49–61, Jan. 1966.
19. Butler, J. and R. Lowe, "Beam-forming matrix simplifies design of electronically scanned antennas," *Electron. Design*, Vol. 9, 170–173, Apr. 1961.
20. Davies, D. E. N., "Application of electronic sector scanning techniques to height-finding radar systems," *Proceedings of the Institution of Electrical Engineers*, Vol. 110, No. 11, 1941–1948, Nov. 1963.
21. Moghaddam, M., Y. Rahmat-Samii, P. Partridge, L. van Nieuwstadt, J. Vitaz, M. Haynes, J. Huang, and V. Cable, "Dual polarized UHF/VHF honey COMB stacked-patch feed array for a large-aperture space-borne radar antenna," *2007 IEEE Aerospace Conference*, 1–10, Mar. 3–10, 2007.
22. Allen, C., "Vari-focal reflector design for a stacked-beam antenna," *Antennas and Propagation Society International Symposium, 1975*, Vol. 13, 101–104, Jun. 1975.
23. Yang, G., M. Ali, and R. Dougal, "A multi-functional stacked patch antenna for wireless power beaming and data telemetry," *2005 IEEE Antennas and Propagation Society International Symposium*, Vol. 2A, 359–362, Jul. 3–8, 2005.
24. Byun, W., B.-S. Kim, K.-S. Kim, and M.-S. Song, "Design of switched beam-forming antenna using stacked microstrip patch with cavity and butler matrix for 60 GHz WPAN application," *2007 IEEE Antennas and Propagation Society International Symposium*, 3640, Jun. 9–15, 2007.

25. Daneshmand, M., L. Shafai, and P. Mousavi, "Beam scanning using the stacked microstrip antenna parameters," *2002 IEEE Antennas and Propagation Society International Symposium*, Vol. 2, 10–13, 2002.
26. Blass, J., "Multidirectional antenna — A new approach to stacked beams," *IRE International Convention Record*, Vol. 8, 48–50, Mar. 1966.
27. Gruszczynski, S., K. Wincza, and K. Sachse, "Design of compensated coupled-stripline 3-dB directional couplers, phase shifters and magic-Ts — Part I: Single-section coupled-line circuits," *IEEE Trans. Microw. Theory Tech.*, Vol. 54, No. 11, 3986–3994, Nov. 2006.
28. Wait, J. R., *Electromagnetic Waves in Stratified Media*, IEEE Press, New York, 1996.
29. Davis, V. B., J. T. Williams, D. R. Jackson, S. A. Long, and S. Jiang, "Effect of ground plane size on radiation patterns of reduced surface wave antennas," *IEEE Trans. Antennas Propagat.*, to be published.
30. Bhattacharyya, A. K., "Characteristics of space and surface-waves in amultilayered structure," *IEEE Trans. Antennas Propagat.*, Vol. 38, 1231–1238, Aug. 1990.
31. Michalski, K. A. and D. Zheng, "Electromagnetic scattering and radiation by surfaces of arbitrary shape in layered media — Part I: Theory," *IEEE Trans. Antennas Propagat.*, Vol. 38, 335–344, Mar. 1990.
32. Itoh, T., "Spectral domain immittance approach for dispersion characteristics of generalized printed transmission lines," *IEEE Trans. Microwave Theory Tech.*, Vol. 28, 733–736, Jul. 1980.
33. Foudazi, A. and A. R. Mallahzadeh, "Pattern synthesis for multi-feed reflector antennas using invasive weed optimisation," *IET Microwaves, Antennas & Propagation*, Vol. 6, No. 14, 1583–1589, Nov. 20, 2012.